

 Open access • Journal Article • DOI:10.1111/DOM.13362

Metformin targets brown adipose tissue in vivo and reduces oxygen consumption in vitro — [Source link](#)

Peter Breining, Jonas Jensen, Elias Immanuel Ordell Sundelin, Lars C. Gormsen ...+13 more authors

Institutions: Aarhus University Hospital, Aarhus University, University of Southern Denmark, University of Copenhagen

Published on: 01 Sep 2018 - Diabetes, Obesity and Metabolism (Diabetes Obes Metab)

Topics: Brown adipose tissue and Metformin

Related papers:

- [Targeted Disruption of Organic Cation Transporter 3 Attenuates the Pharmacologic Response to Metformin](#)
- [Role of AMP-activated protein kinase in mechanism of metformin action](#)
- [Antihyperglycemic mechanism of metformin occurs via the AMPK/LXR \$\alpha\$ /POMC pathway.](#)
- [Metformin: From Mechanisms of Action to Therapies](#)
- [Beneficial effects of metformin on energy metabolism and visceral fat volume through a possible mechanism of fatty acid oxidation in human subjects and rats.](#)

Share this paper:    

View more about this paper here: <https://typeset.io/papers/metformin-targets-brown-adipose-tissue-in-vivo-and-reduces-3s73dp1t3b>

Metformin targets brown adipose tissue in vivo and reduces oxygen consumption in vitro

Breining, Peter; Jensen, Jonas B; Sundelin, Elias I; Gormsen, Lars C; Jakobsen, Steen; Busk, Morten; Rolighed, Lars; Bross, Peter; Fernandez-Guerra, Paula; Markussen, Lasse K; Rasmussen, Nanna E; Hansen, Jacob B.; Pedersen, Steen B; Richelsen, Bjørn; Jessen, Niels

Published in:
Diabetes, Obesity and Metabolism

DOI:
10.1111/dom.13362

Publication date:
2018

Document version:
Accepted manuscript

Citation for published version (APA):
Breining, P., Jensen, J. B., Sundelin, E. I., Gormsen, L. C., Jakobsen, S., Busk, M., Rolighed, L., Bross, P., Fernandez-Guerra, P., Markussen, L. K., Rasmussen, N. E., Hansen, J. B., Pedersen, S. B., Richelsen, B., & Jessen, N. (2018). Metformin targets brown adipose tissue in vivo and reduces oxygen consumption in vitro. *Diabetes, Obesity and Metabolism*, 20(9), 2264-2273. <https://doi.org/10.1111/dom.13362>

Go to publication entry in University of Southern Denmark's Research Portal

Terms of use

This work is brought to you by the University of Southern Denmark.
Unless otherwise specified it has been shared according to the terms for self-archiving.
If no other license is stated, these terms apply:

- You may download this work for personal use only.
- You may not further distribute the material or use it for any profit-making activity or commercial gain
- You may freely distribute the URL identifying this open access version

If you believe that this document breaches copyright please contact us providing details and we will investigate your claim.
Please direct all enquiries to puresupport@bib.sdu.dk

AUTHORS AND AFFILIATIONS

Peter Breining^{1,2*}, Jonas B. Jensen^{3*}, Elias I. Sundelin³, Lars C. Gormsen⁴, Steen Jakobsen⁴, Morten Busk⁵, Lars Rolighed⁶, Peter Bross⁷, Paula Fernandez-Guerra⁷, Lasse K. Markussen^{8,9}, Nanna E. Rasmussen⁸, Jacob B. Hansen⁸, Steen B. Pedersen¹, Bjørn Richelsen¹, Niels Jessen^{2,3,10}

*Peter Breining and Jonas B. Jensen should be considered joint first author

1 Department of Endocrinology and Internal Medicine, Aarhus University Hospital, Denmark

2 Department of Clinical Pharmacology, Aarhus University Hospital, Denmark

3 Department of Clinical Medicine - Research Laboratory for Biochemical Pathology, Aarhus University, Aarhus, Denmark

4 Department of Nuclear Medicine and PET Center, Aarhus University Hospital, Aarhus, Denmark

5 Department of Experimental Clinical Oncology, Aarhus University Hospital, Denmark

6 Department of Otorhinolaryngology and Department of Surgery P, Aarhus University Hospital, Denmark

7 Department of Clinical Medicine - Research Unit for Molecular Medicine, Aarhus University and Aarhus University Hospital, Denmark

8 Department of Biology, University of Copenhagen, Denmark

9 Department of Biochemistry and Molecular Biology, University of Southern Denmark, Denmark

10 Department of Biomedicine, Aarhus University, Denmark

CORRESPONDING AUTHOR

This article has been accepted for publication and undergone full peer review but has not been through the copyediting, typesetting, pagination and proofreading process, which may lead to differences between this version and the Version of Record. Please cite this article as doi: 10.1111/dom.13362

Professor Niels Jessen, MD, PhD

Department of Biomedicine, Aarhus University Hospital

Wilhelm Meyers Alle 4, DK-8000 Aarhus C, Denmark

Niels.jessen@biomed.au.dk

Telephone number: +4587167569, E-mail address: niels.jessen@biomed.au.dk

ABSTRACT

Metformin is the most widely prescribed oral antidiabetic drug worldwide. Despite well-documented beneficial effects on health outcomes in diabetic patients, the target organs that mediate the effects of metformin remain to be established. In adult humans, brown adipose tissue (BAT) can influence basic metabolic rate, making BAT an attractive target for treatment of type 2 diabetes. Under the hypothesis that BAT is a metformin target tissue, we investigated *in vivo* uptake of [^{11}C]-metformin tracer in mice and studied *in vitro* effects of metformin on cultured human brown adipocytes. Injected [^{11}C]-metformin revealed avid uptake in the murine interscapular BAT depot. Metformin exposure in BAT was comparable to hepatic exposure. Non-specific inhibition of the organic cation transporter (OCT) protein by cimetidine administration eliminated BAT exposure to metformin, demonstrating OCT mediated uptake. Gene expression profiles of OCTs in BAT revealed ample OCT3 expression in both human and mouse BAT. Incubation of a human brown adipocyte cell models with metformin reduced cellular oxygen consumption in a dose dependent manner. Collectively, these results support BAT as a putative metformin target.

Metformin has been used in the treatment of type 2 diabetes for more than half a century and is currently the recommended first-line oral antidiabetic drug worldwide. Metformin treatment improves glycemic control and reduces cardiovascular mortality without weight gain or risk of hypoglycemia [1, 2]. However, despite its common use, the mechanisms of action of metformin remain to be fully established. In subjects with type 2 diabetes, metformin treatment can reduce hepatic glucose production [3-5], but this finding has not been consistently observed [6, 7], and in healthy non-diabetic subjects, metformin treatment increases hepatic glucose production [8, 9]. Investigations of metformin mediated effects on glucose disposal are also inconclusive with some results showing a positive effect [6, 10] while other show no increase in glucose disposal [11, 12]. This has led to speculations whether the effect of metformin involves target organs besides liver and skeletal muscle. This notion is supported by evidence of direct effects of metformin on gut hormones [13, 14] and the microbiome [15].

Metformin targets intracellular effectors leading to suppression of mitochondrial function [16-18]. Because the drug is hydrophilic, it relies on carrier proteins for cellular uptake. These proteins involve members of the organic cation transporter (OCT) family, Plasma membrane monoamine transporter (PMAT), and Multidrug and toxin extrusion protein 1 (MATE1) [19]. PMAT is found on the luminal side of enterocytes in the intestines and may be the main transporter responsible for metformin uptake from the gastrointestinal tract [19]. OCT1 is mainly present in the liver, OCT2 is primarily found in the kidney [19, 20] whereas OCT3 is ubiquitously expressed to a variable extent throughout the body [21]. MATE1 is found in multiple organs and is thought to be responsible for metformin excretion in e.g. liver and kidney cells [19]. Metformin is not metabolized *in vivo* but is eliminated through OCT2 and MATE1 in the kidneys [19].

Brown adipose tissue (BAT) is a metabolically highly active organ, which has been proposed as a target in the treatment and prevention of type 2 diabetes and obesity [22]. Brown adipocytes are

capable of dissipating chemically bound energy as heat through uncoupling of the respiratory chain by the action of uncoupling protein 1 (UCP1), a protein unique to these cells [23]. In mice, metformin treatment is associated with increased VLDL clearance in BAT [24] and increments in proteins involved in mitochondrial biogenesis. These observations could indicate a direct action of metformin on BAT. This is further supported by the detection of metformin in BAT shortly after IV administration of the drug [16], and increases in gene expression of BAT-associated proteins, UCP1 and ELOVL3, in peritoneal visceral fat during metformin treatment [25]. However, if metformin mediates this effect through direct action on the tissue is still to be investigated.

We have recently demonstrated how [^{11}C]-metformin Positron Emission Tomography (PET) is a novel and robust method of studying pharmacokinetic properties of metformin in both animals and humans [20, 26]. Under the hypothesis that metformin directly targets BAT, we have investigated biodistribution of metformin in mice *in vivo* and assessed potential effects of metformin on human UCP1 positive adipocytes *in vitro*.

RESEARCH DESIGN AND METHODS

Animals

Mice were purchased from Taconic, Denmark. All animals were group housed with free access to water and standard chow until the study day. Cages were kept at room temperature (20-22 degrees Celsius) in a humidity-controlled environment with a 12-h light/dark cycle.

The studies were approved by the Animal Experiments Inspectorate and performed in accordance with the Danish Animal Experimentation act.

Radiochemistry

[¹¹C]-Metformin (0.2–1.0 GBq) containing 0.1–0.5 µg/mL metformin was synthesized as previously published [26]. Each production was tested and all were >98% pure.

[¹¹C]-metformin MicroPET/MRI

Wild-type and corresponding *Oct1/2^{-/-}* mice on a FVB background [27] (aged 13–15 weeks) underwent functional PET and anatomical MRI scanning using Mediso nanoScan PET/MR (Mediso Medical Imaging Systems) as previously described [28]. Anesthesia was induced using 5% isoflurane and maintained with mask-delivered isoflurane (1.8–2.0%). A bolus of [¹¹C]-metformin (5.7 ± 2.8 MBq/animal) was injected through a tail vein catheter, followed by 60-minutes of dynamic PET and 30-min MRI. A heating pad maintained body temperature from declining and respiration frequency was monitored. To non-selectively inhibit OCT function, mice were pharmacologically pretreated with Cimetidine (150 mg/kg). Specific inhibition of MATE1 was obtained by pyrimethamine (5 mg/kg) administration in a separate experiment. Control mice were intravenously pretreated with a corresponding vehicle in an equal volume. Pre-treatments were administered 5 minutes prior to [¹¹C]-Metformin injection.

The reconstructing protocol has been published previously [28]. In short, 60 min dynamic PET-scans were reconstructed with increasing duration from 5 seconds to 10 minutes (30 frames in all). PMOD version 3.5 (PMOD Technologies Ltd) was used for imaging analysis. Multiple regions of interest (ROIs) were placed on coronal slices in the organ of interest creating a volume of interest (VOI). A blood VOI was generated by averaging images from the first 20 sec over the blood-pool in the left ventricle. A BAT VOI was placed as a cylinder (71 µL) covering the interscapular BAT depot, on PET-images averaged from 0-30 min. A hepatic VOI was drawn in the anterior part of the

liver on PET-images averaged from 0-15 min. Positioning of all VOIs was controlled in each time frame. MR-images were used for defining size and demarcation of the liver, heart and interscapular area.

Time-activity curves from the liver, blood and BAT were generated from the individual VOIs, and data were expressed as tissue-to-blood ratio by dividing the tissue concentration of [^{11}C]-metformin by the blood concentration at each time point for each animal. Area under the curve (AUC) of the tissue-to-blood ratio curve reflects the tissue extraction ratio [29] and thereby the relationship between uptake and elimination.

Distribution of metformin 60 min after IV-administration

Six unanaesthetized C57BL/6 mice (aged 15-18 weeks) were administered a bolus [^{11}C]-Metformin (5.4 ± 3.7 MBq) through a tail vein catheter. After 60 minutes, anesthesia was induced using 5% isoflurane. Blood was sampled from the retrobulbar venous plexus and the mice were sacrificed by cervical dislocation. BAT, epididymal AT, inguinal subcutaneous AT, retroperitoneal AT, liver, kidney, heart, ilium (approximately 5 cm proximal to the caecum) and colon were harvested, rinsed, weighed and added to RNAlater (Sigma-Aldrich). Tissue radioactivity was determined using a Packard Gamma Counter (Packard Cobra Auto-Gamma) and expressed relative to blood radioactivity. All measurements were corrected for decay and data are expressed as the tissue-to-blood ratio.

Human deep neck adipose tissue biopsies

Human adipose tissue (AT) biopsies from the subcutaneous neck AT and deep-neck AT were collected during elective surgery as previously described [30]. None of the study participants had diabetes nor were they administered β -adrenergic antagonists. All biopsies were collected in a period from late January until the middle of March 2015. Each participant had one subcutaneous AT biopsy taken and one to three deep-neck AT. This resulted in a total of 12 subcutaneous AT biopsies and 24 deep-neck AT biopsies that were instantly frozen in liquid nitrogen. All study participants gave informed written consent. The study was approved by the Central Denmark Region ethics committee and was performed in accordance with the Declaration of Helsinki.

RNA isolation and Quantitative Real-Time PCR

Total RNA from all dissected tissues was isolated with TRIzol reagent (Ambion, Life Technologies). The cDNA was synthesized using random hexamer primers by the Verso cDNA Kit (Applied Biosystems, Life Technologies). All analyses were performed in duplicates using the “SYBR Green I Master” (Roche Life Science) in a LightCycler 480 (Roche Life Science). The default “advanced relative quantification” mode (software version LCS 480 1.5.0.39, Roche Applied Science) estimated the relative gene expression. Multiple reference genes were tested for stability and Peptidylprolyl isomerase A (cyclophilin A) (PPIA) was found superior when comparing fat tissues. Target gene levels are expressed relative to PPIA. The PCR Protocol used was: 10s at 95°C, 20s at 60°C and 10s at 72°C. The increase in fluorescence was measured in real time during the extension step.

In vitro oxygen consumption and extracellular acidification measurements

Immortalized brown adipocytes of human origin (TERT-hBA), passage 10-12 were cultured as previously described [31]. At day nine of differentiation, cells were replated into gelatin-covered 96-well XF Cell Culture Microplates (20,000 cells/well). Cells were kept in growth medium (Advanced DMEM/F12) supplemented with 2 % FBS, penicillin (62.5 µg/ml), streptomycin (100 µg/ml), L-glutamine (2 mM) and T3 (1 nM) for two days. Immortalized white adipocytes of human origin (TERT-hWA) [31], passage 12-13, and hMADS cells [32] were cultured as described [31]. At day nine of differentiation, cells were replated as described above. Cells were kept in growth medium without T3. At day 12, cells were treated with rosiglitazone (1 µM) to induce browning [31]. Analyses were conducted at day 15. Twenty-four h before the analyses, the medium was changed to growth medium supplemented with rosiglitazone (1 µM) and metformin (0, 0.1 or 0.5 mM). One hour before the analyses, the medium was changed to Seahorse basal medium (Agilent Technologies) supplemented with 5 mM glucose, 1 mM pyruvate, 2 mM glutamine, adjusted to pH 7.4 ± metformin. 60 min before first measurement plates were incubated in a non-CO₂ incubator. Basal OCR was assessed at the last measurement before chemical uncoupling by 1.0 µM Carbonyl cyanide-4-(trifluoromethoxy)phenylhydrazone (FCCP). Maximal respiratory capacity was assessed at the last measurement before inhibition of the respiratory chain by rotenone (0.5 µM) and antimycin A (0.5 µM). At all time-points, OCR was established as a mean of the measurements from 10-15 wells after discarding technical outliers.

For gene expression analysis, three separate plates of TERT-hBA cells were differentiated and snap frozen in liquid nitrogen at day 11.

Statistical Analyses

Data distribution was assessed by qq-plots. When uneven distribution was identified, data was logarithmically transformed to obtain a normal distribution. The murine data were compared using the Student's t test or ANOVA with Bonferroni's correction for multiple comparisons (Post hoc analysis) and expressed as mean \pm SE. When assessing human biopsy material, intrapersonal dependence was taken into account by clustering standard error on the level of the individual [30]. Cell intervention analyses within the same passage were compared by paired t-test. A P-value of <0.05 was considered statistically significant. Statistical analyses were performed using GraphPad Prism 5.01 for windows and STATA 13.1 for windows.

RESULTS

Metformin is distributed to BAT in mice *in vivo*

Intravenous administration of [^{11}C]-metformin in mice revealed avid uptake in the interscapular BAT depot (Fig 1). The surrounding region did not add to the signal, as the [^{11}C] signal was isolated to the BAT (Fig 1 A+D). The AUC of metformin tissue-to-blood ratio during the first hour after IV administration (AUC) in BAT was comparable to liver (Fig 1B+C). The distribution pattern differed markedly between BAT and liver with a time to maximum tissue concentration (T_{max}) of the tissue-to-blood ratio in the liver after approximately 3.5 minutes (Fig 1,B) whereas uptake in BAT was still increasing at $T=60$ minutes. Tissue levels of metformin at $t=60$ minutes determined by Gamma Counter confirmed the findings by microPET (Fig 1D). Metformin content per gram of tissue was higher in BAT compared to other adipose tissue depots and heart, and comparable to kidney and intestines (Fig. 1D).

Non-specific OCT inhibition by pretreatment with cimetidine almost completely ablated metformin distribution to BAT (Fig 2A). A minor 1.4-fold reduction in AUC was seen in *Oct1/2*^{-/-} mice (Fig

2B) within the first hour of administration. Inhibition of MATE1 after pyrimethamine injection was associated with a slight reduction in metformin distribution to BAT, but this did not reach statistical significance.

OCT3 gene expression is enriched in brown adipose tissue from mice and humans

To test if the gene expression profile of metformin transporter proteins in BAT is similar in mice and humans, adipose tissue was collected from both species. In mice, adipose tissue from the interscapular and inguinal depots was dissected and analyzed for *Ucp1* gene expression. As expected *Ucp1* expression was high in the interscapular depot and barely detectable in the subcutaneous inguinal adipose depot, (Fig 3A) thereby demonstrating the classic location of BAT in mice.

In humans, deep-neck AT biopsies from study subjects undergoing elective neck surgery were assessed. The subject characteristics are shown in Table 1. Expression of *UCP1* in human deep-neck AT showed a large degree of heterogeneity, ranging from undetectable UCP1 mRNA to levels comparable to those found in murine BAT (Fig 3A). Gene expression profiling of metformin transporters revealed that *SLC22A3*, encoding OCT3, is the most abundantly expressed transporter in murine and human adipose tissue (Fig 3B+C). In the human brown adipocyte cell model (TERT-hBA), gene expression analysis revealed a low *SLC22A1-3* expression, encoding OCT1-3, whereas *SLC47A1* expression, encoding MATE1, was comparable to human AT (Fig 3C).

Metformin inhibits cellular respiration in human beige and brown adipocyte cell models

Dose-response assessments of TERT-hBA cells during a short-term 60 min pre-incubation with 0.1 to 2 mM metformin revealed dose-dependent reductions in oxygen consumption rate (OCR) (Fig 4A). There were no clear differences in extracellular acidification rates (ECAR) between the treatments (Fig 4B) under these conditions. Pre-incubation with 1 mM metformin for 60 min inhibited cellular oxygen consumption by 11.1% ($P=0.01$, CI 6.4;15.8) during basal conditions and 7.0% after chemical uncoupling with FCCP ($P=0.08$, CI -2.2;16.1) (Fig 4C), but did not affect extracellular acidification rate (Fig 4D).

Next, we studied cellular respiration after prolonged exposure (24 hours) to 0.1 and 0.5 mM metformin in two additional human thermogenic cell models (TERT-hWA and hMADS). Both cell-lines were “browned” by treatment with rosiglitazone from days 12-15 as described previously [31]. Oxygen consumption in hMADS cell model was reduced by 9% during incubation with 0.1 mM metformin ($P<0.01$) and by 42% during incubation with 0.5 mM metformin ($P=0.03$) (Fig 5A). Similar to short-term exposure, OCR was also reduced by metformin during chemical uncoupling (Fig 5A). As shown in Fig 5B, metformin had similar effects in TERT-hWA cells. During prolonged exposure to 0.5 mM metformin, ECAR increased by 39% increase in the hMADS cell line ($P<0.01$) and 33% in the TERT-hWA cell model (Fig 5C+D) while no effect on ECAR by 0.1 mM metformin was observed.

DISCUSSION

This study demonstrates that metformin targets BAT *in vivo* in rodents through organic cation transporter-mediated uptake. Previous studies have demonstrated abundant uptake of metformin in liver, kidneys, salivary glands and the intestinal mucosa [14] while small amounts of metformin may be transported into white adipose tissue and muscle [16, 33]. The metformin exposure in BAT

demonstrated in this study was comparable in magnitude to exposure in the liver, a well-established metformin target organ [19]. Metformin may therefore directly target substrate metabolism in BAT.

The pharmacokinetic profile of metformin in BAT does not resemble hepatic distribution. Similar to the liver, the interscapular BAT is highly vascularized [34] suggesting that the difference in metformin distribution is not solely explained by differences in vascularization. Instead, the difference in the pharmacokinetic profile can be a consequence of a difference in transporter protein profiles between the two tissues. The pronounced reduction in uptake of metformin in BAT during co-administration with cimetidine demonstrates that metformin uptake in BAT indeed depends on normal function of transporter proteins. The half-maximal inhibitory concentrations (IC₅₀) of cimetidine on OCT1, OCT2, and OCT3 are comparable [35], and administration of cimetidine does therefore not provide evidence for which OCT-isoform is involved. The minute effect of combined ablation of OCT1 and OCT2 and the results from the gene expression studies suggests that OCT3 is likely facilitating uptake of metformin into BAT. The capacity of OCT3 to transport metformin in selected tissues is evident in OCT3^{-/-} mice where accumulation of metformin in salivary glands is abolished [36]. OCT3 is widely expressed in multiple tissues [21], and interestingly, OCT3 knockout is associated with attenuated response to metformin treatment [21]. This demonstrates that at least some of the pharmacodynamic actions of metformin are mediated through this transporter. However, this study does not provide direct evidence that OCT3 is the mediator of metformin uptake in BAT, and the involvement of other transporter proteins cannot be excluded.

We have previously determined whole body metformin distribution in four healthy human subjects *in vivo* [20]. In these subjects, we detected marginal uptake of metformin in the neck area, which was predominantly confined to the parotid glands, a well-known target organ of metformin [36]. However, BAT presence was not determined in the study subjects [37]. Unlike rodents, brown adipocytes in humans are typically scattered within large depots of white adipose tissue. There is

substantial interpersonal variation in BAT amount [37], but BAT is often enriched in the deep-neck AT [37]. Direct investigations of [^{14}C]-metformin uptake in human BAT, therefore, require determination of BAT location in a separate scan, e.g., using FDG-PET during cold-exposure [37]. Although not providing direct evidence of metformin uptake in human BAT, the gene expression profile of UCP1-containing adipocytes from deep-neck AT in humans suggests that metformin uptake in human BAT is likely. OCT3 is encoded by the *SLC22A3* gene, and it is the most abundantly expressed metformin transporter in human deep-neck AT, and *UCP1* and *SLC22A3* gene expression levels closely correlate in human deep-neck AT [30].

Several lines of evidence imply that metformin inhibits complex-1 in the inner mitochondrial membrane [17, 18], and thereby reduces substrate oxidation [18]. This aligns with the reduced oxygen consumption rate in TERT-hBA cells observed in this study, and by observations in mice where treatment with metformin increases both expression and activation of AMPK in BAT [24]. Metformin action on BAT may not necessarily be confined to inhibition of mitochondrial function but may also interact with OCT activity. OCT3 functions as a contributing regulator of extracellular catecholamine levels by facilitating local removal of endogenous amines. Metformin is a competitive substrate of OCT transport [38] and may thereby increase beta-adrenergic receptor stimulation in BAT. In rodents, norepinephrine stimulation of brown preadipocytes and mature adipocytes will lead to recruitment in brown adipose tissue [39]. This mechanism may translate to humans because increases in BAT mass and activity have been observed in patients with pheochromocytoma and paraganglioma [33, 40]. Interestingly, metformin treatment of immortalized murine brown adipocytes acutely increases p44/p42 mitogen-activated protein kinase (MAPK) activation and reduces leptin secretion [41]. In addition, metformin treatment may rescue obesity-induced suppression of brown adipogenesis and thermogenesis [42]. Also, two weeks of daily metformin administration to rats increases *Ucp1* expression in the post-prandial state [43] and

14 weeks of daily metformin administration increases expression of genes associated with BAT in mice [25]. Hence, metformin action on BAT may assert both acute and more prolonged effects on BAT function.

Metformin levels in plasma varies greatly among diabetes patients under controlled conditions [44]. Therapeutic levels have been suggested to be between 0.7 and 7 μM [45], but consensus has not been established [46]. During clinical use, plasma metformin levels between 0 and 113 mg/L (868 μM) have been measured in random blood samples from diabetic subjects [47]. The decrease in cellular respiration in TERT-hBA cells during short-term metformin exposure was observed using high to supra-pharmacological metformin concentrations. As demonstrated in our gene-expression profiles, the gene expression levels of *SLC22A3* in TERT-hBA cells were more than 10-fold lower compared to adipose tissue from the human deep neck. Therefore, to facilitate cellular uptake during *in vitro* conditions high concentration of metformin was necessary. The increased ratio of *SLC47A1* (MATE1) to *SLC22A3* (OCT3) expression may also be a contributing factor to a low uptake of metformin in TERT-hBA cells as MATE1 facilitates excretion of metformin from the cell [48]. Concentrations of 1 mM or higher is often used for *in vitro* studies [18, 49] but to study the effects of metformin in human brown adipocytes under conditions better resembling the *in vivo* situation, we chose a lower concentration and a longer exposure time. Furthermore, to test if the effects of metformin were confined to only TERT-hBA cells, we used two additional cell models with a different metformin transporter transcription profile. Importantly, in one of these (hMADS) transcription of the efflux-transporter, MATE1, is low [50]. In both hMADS and TERT-hWA, metformin decreased oxygen consumption in 0.1 mM concentrations. In addition, prolonged exposure to metformin increased ECAR which may be due to increased glycolytic rate or increased CO_2 production[51]. These *in vitro* demonstrate direct cellular effects of metformin in cells expressing UCP1, but the direct effects of metformin in BAT in human remain to be established.

In conclusion, our data demonstrate that OCTs facilitate avid uptake of metformin in mouse BAT *in vivo*. This finding may be translated to humans as gene expression profiles of metformin transporter proteins in BAT are conserved between species. In immortalized brown adipocytes of human origin, metformin decreases cellular respiration and hence support a direct pharmacological action of the drug in BAT. Collectively, the data suggest that BAT is a potential target organ of metformin action.

Acknowledgements

Tissue samples from OCT3-KO mice were generously donated from Kathleen M. Giacomini and her team at the University of California, San Francisco. We thank Dr. Christian Dani for the kind gift of hMADS cells. We thank Helle Zibrandtsen, Pia Hornbek and Lenette Pedersen for their excellent technical laboratory assistance.

Funding.

This work was supported by a Novo Nordisk Foundation Excellence Project grant to N.J, the Danish Council for Independent Research (Det Frie Forskningsråd) (grant DFF-4183-00384), the Department of Clinical Medicine, Aarhus University and the AP Møller Foundation.

No potential conflicts of interest relevant to this article were reported.

Author Contributions

P.B., J.B.J., B.R. and N.J. participated in designing the study. P.B., J.B.J., E.I.S., S.J., P.F.G, N.E.R, L.K.M, M.B and L.R. conducted experiments and analyzed the data. P.B., J.B.J. and N.J. contributed to writing the manuscript. S.B.P., B.R., Bross, J.H, L.C.G. reviewed/edited the manuscript.

N.J. is the guarantor of this work and, as such, had full access to all the data in the study and takes responsibility for the integrity of the data and the accuracy of the data analysis. Preliminary results have been presented at the “52nd Annual Meeting of the Scandinavian Society for the Study of Diabetes” and at the “13th Congress of the European Association for Clinical Pharmacology and Therapeutics”.

Reference List

- [1] Inzucchi SE, Maggs DG, Spollett GR, *et al.* Efficacy and metabolic effects of metformin and troglitazone in type II diabetes mellitus. *N Engl J Med.* 1998; **338**: 867-872
- [2] Abbasi F, Chu JW, McLaughlin T, Lamendola C, Leary ET, Reaven GM. Effect of metformin treatment on multiple cardiovascular disease risk factors in patients with type 2 diabetes mellitus. *Metabolism.* 2004; **53**: 159-164
- [3] Hundal RS, Krssak M, Dufour S, *et al.* Mechanism by which metformin reduces glucose production in type 2 diabetes. *Diabetes.* 2000; **49**: 2063-2069
- [4] Stumvoll M, Nurjhan N, Perriello G, Dailey G, Gerich JE. Metabolic effects of metformin in non-insulin-dependent diabetes mellitus. *New England Journal of Medicine.* 1995; **333**: 550-554
- [5] Johnson A, Webster J, Sum C-F, *et al.* The impact of metformin therapy on hepatic glucose production and skeletal muscle glycogen synthase activity in overweight type II diabetic patients. *Metabolism.* 1993; **42**: 1217-1222
- [6] Hother-Nielsen O, Schmitz O, Andersen PH, Beck-Nielsen H, Pedersen O. Metformin improves peripheral but not hepatic insulin action in obese patients with type II diabetes. *Acta endocrinologica.* 1989; **120**: 257-265
- [7] Nosadini R, Avogaro A, Trevisan R, *et al.* Effect of metformin on insulin-stimulated glucose turnover and insulin binding to receptors in type II diabetes. *Diabetes Care.* 1987; **10**: 62-67
- [8] Christensen MMH, Højlund K, Hother-Nielsen O, *et al.* Endogenous glucose production increases in response to metformin treatment in the glycogen-depleted state in humans: a randomised trial. *Diabetologia.* 2015; **58**: 2494-2502
- [9] Konopka AR, Esponda RR, Robinson MM, *et al.* Hyperglucagonemia mitigates the effect of metformin on glucose production in prediabetes. *Cell reports.* 2016; **15**: 1394-1400
- [10] Zhou G, Myers R, Li Y, *et al.* Role of AMP-activated protein kinase in mechanism of metformin action. *J Clin Invest.* 2001; **108**: 1167-1174
- [11] Perriello G, Misericordia P, Volpi E, *et al.* Acute antihyperglycemic mechanisms of metformin in NIDDM: evidence for suppression of lipid oxidation and hepatic glucose production. *Diabetes.* 1994; **43**: 920-928
- [12] DEFRONZO RA, Barzilai N, SIMONSON DC. Mechanism of metformin action in obese and lean noninsulin-dependent diabetic subjects. *The Journal of Clinical Endocrinology & Metabolism.* 1991; **73**: 1294-1301
- [13] Bailey C, Mynett K, Page T. Importance of the intestine as a site of metformin - stimulated glucose utilization. *British journal of pharmacology.* 1994; **112**: 671-675
- [14] McCreight LJ, Bailey CJ, Pearson ER. Metformin and the gastrointestinal tract. *Diabetologia.* 2016; **59**: 426-435
- [15] Forslund K, Hildebrand F, Nielsen T, *et al.* Disentangling type 2 diabetes and metformin treatment signatures in the human gut microbiota. *Nature.* 2015; **528**: 262-266
- [16] Madiraju AK, Erion DM, Rahimi Y, *et al.* Metformin suppresses gluconeogenesis by inhibiting mitochondrial glycerophosphate dehydrogenase. *Nature.* 2014; **510**: 542-546
- [17] El-Mir MY, Nogueira V, Fontaine E, Averet N, Rigoulet M, Leverve X. Dimethylbiguanide inhibits cell respiration via an indirect effect targeted on the respiratory chain complex I. *J Biol Chem.* 2000; **275**: 223-228
- [18] Owen MR, Doran E, Halestrap AP. Evidence that metformin exerts its anti-diabetic effects through inhibition of complex 1 of the mitochondrial respiratory chain. *The Biochemical journal.* 2000; **348 Pt 3**: 607-614
- [19] Todd JN, Florez JC. An update on the pharmacogenomics of metformin: progress, problems and potential. *Pharmacogenomics.* 2014; **15**: 529-539

- [20] Gormsen LC, Sundelin EI, Jensen JB, *et al.* In Vivo Imaging of Human ¹¹C-Metformin in Peripheral Organs: Dosimetry, Biodistribution, and Kinetic Analyses. *Journal of Nuclear Medicine*. 2016; **57**: 1920-1926
- [21] Chen EC, Liang X, Yee SW, *et al.* Targeted disruption of organic cation transporter 3 attenuates the pharmacologic response to metformin. *Mol Pharmacol*. 2015; **88**: 75-83
- [22] Chondronikola M, Volpi E, Borsheim E, *et al.* Brown Adipose Tissue Improves Whole Body Glucose Homeostasis and Insulin Sensitivity in Humans. *Diabetes*. 2014; **63**: 4089-4099
- [23] Cannon B, Nedergaard J. Brown adipose tissue: function and physiological significance. *Physiol Rev*. 2004; **84**: 277-359
- [24] Geerling JJ, Boon MR, van der Zon GC, *et al.* Metformin lowers plasma triglycerides by promoting VLDL-triglyceride clearance by brown adipose tissue in mice. *Diabetes*. 2014; **63**: 880-891
- [25] Kim EK, Lee SH, Jhun JY, *et al.* Metformin Prevents Fatty Liver and Improves Balance of White/Brown Adipose in an Obesity Mouse Model by Inducing FGF21. *Mediators of inflammation*. 2016; **2016**:
- [26] Jakobsen S, Busk M, Jensen JB, *et al.* A PET Tracer for Renal Organic Cation Transporters, (1)(1)C-Metformin: Radiosynthesis and Preclinical Proof-of-Concept Studies. *J Nucl Med*. 2016; **57**: 615-621
- [27] Jonker JW, Wagenaar E, Van Eijl S, Schinkel AH. Deficiency in the organic cation transporters 1 and 2 (Oct1/Oct2 [Slc22a1/Slc22a2]) in mice abolishes renal secretion of organic cations. *Mol Cell Biol*. 2003; **23**: 7902-7908
- [28] Jensen JB, Sundelin EI, Jakobsen S, *et al.* [¹¹C]-metformin distribution in the liver and small intestine using dynamic PET in mice demonstrates tissue-specific transporter dependency. *Diabetes*. 2016; **65**: 1724-1730
- [29] Testa A, Zanda M, Elmore CS, Sharma P. PET Tracers To Study Clinically Relevant Hepatic Transporters. *Mol Pharm*. 2015; **12**: 2203-2216
- [30] Breining P, Pedersen SB, Pikelis A, *et al.* High expression of organic cation transporter 3 in human BAT-like adipocytes. Implications for extraneuronal norepinephrine uptake. *Mol Cell Endocrinol*. 2017; **443**: 15-22
- [31] Markussen LK, Isidor MS, Breining P, *et al.* Characterization of immortalized human brown and white pre-adipocyte cell models from a single donor. *PloS one*. 2017; **12**: e0185624
- [32] Rodriguez AM, Pisani D, Dechesne CA, *et al.* Transplantation of a multipotent cell population from human adipose tissue induces dystrophin expression in the immunocompetent mdx mouse. *The Journal of experimental medicine*. 2005; **201**: 1397-1405
- [33] Sondergaard E, Gormsen LC, Christensen MH, *et al.* Chronic adrenergic stimulation induces brown adipose tissue differentiation in visceral adipose tissue. *Diabet Med*. 2015; **32**: e4-e8
- [34] Rothwell NJ, Stock MJ. Influence of noradrenaline on blood flow to brown adipose tissue in rats exhibiting diet-induced thermogenesis. *Pflügers Archiv European Journal of Physiology*. 1981; **389**: 237-242
- [35] Koepsell H, Lips K, Volk C. Polyspecific organic cation transporters: structure, function, physiological roles, and biopharmaceutical implications. *Pharm Res*. 2007; **24**: 1227-1251
- [36] Lee N, Duan H, Hebert MF, Liang CJ, Rice KM, Wang J. Taste of a pill: organic cation transporter-3 (OCT3) mediates metformin accumulation and secretion in salivary glands. *J Biol Chem*. 2014; **289**: 27055-27064
- [37] Cypess AM, Lehman S, Williams G, *et al.* Identification and importance of brown adipose tissue in adult humans. *N Engl J Med*. 2009; **360**: 1509-1517
- [38] Kimura N, Masuda S, Katsura T, Inui K-i. Transport of guanidine compounds by human organic cation transporters, hOCT1 and hOCT2. *Biochemical pharmacology*. 2009; **77**: 1429-1436
- [39] Bouillaud F, Ricquier D, Mory G, Thibault J. Increased level of mRNA for the uncoupling protein in brown adipose tissue of rats during thermogenesis induced by cold exposure or norepinephrine infusion. *The Journal of biological chemistry*. 1984; **259**: 11583-11586

- [40] Frontini A, Vitali A, Perugini J, *et al.* White-to-brown transdifferentiation of omental adipocytes in patients affected by pheochromocytoma. *Biochim Biophys Acta*. 2013; **1831**: 950-959
- [41] Klein J, Westphal S, Kraus D, *et al.* Metformin inhibits leptin secretion via a mitogen-activated protein kinase signalling pathway in brown adipocytes. *The Journal of endocrinology*. 2004; **183**: 299-307
- [42] Yang Q, Liang X, Sun X, *et al.* AMPK/alpha-Ketoglutarate Axis Dynamically Mediates DNA Demethylation in the Prdm16 Promoter and Brown Adipogenesis. *Cell Metab*. 2016; **24**: 542-554
- [43] Tokubuchi I, Tajiri Y, Iwata S, *et al.* Beneficial effects of metformin on energy metabolism and visceral fat volume through a possible mechanism of fatty acid oxidation in human subjects and rats. *PLoS one*. 2017; **12**: e0171293
- [44] Christensen MM, Brasch-Andersen C, Green H, *et al.* The pharmacogenetics of metformin and its impact on plasma metformin steady-state levels and glycosylated hemoglobin A1c. *Pharmacogenet Genomics*. 2011; **21**: 837-850
- [45] Schulz M, Iwersen-Bergmann S, Andresen H, Schmoldt A. Therapeutic and toxic blood concentrations of nearly 1,000 drugs and other xenobiotics. *Critical care*. 2012; **16**: R136
- [46] Kajbaf F, De Broe ME, Lalau JD. Therapeutic Concentrations of Metformin: A Systematic Review. *Clin Pharmacokinet*. 2016; **55**: 439-459
- [47] Lalau JD, Lemaire-Hurtel AS, Lacroix C. Establishment of a database of metformin plasma concentrations and erythrocyte levels in normal and emergency situations. *Clinical drug investigation*. 2011; **31**: 435-438
- [48] Toyama K, Yonezawa A, Masuda S, *et al.* Loss of multidrug and toxin extrusion 1 (MATE1) is associated with metformin - induced lactic acidosis. *British journal of pharmacology*. 2012; **166**: 1183-1191
- [49] Grisouard J, Timper K, Radimerski TM, *et al.* Mechanisms of metformin action on glucose transport and metabolism in human adipocytes. *Biochemical pharmacology*. 2010; **80**: 1736-1745
- [50] Barquissau V, Beuzelin D, Pisani DF, *et al.* White-to-brite conversion in human adipocytes promotes metabolic reprogramming towards fatty acid anabolic and catabolic pathways. *Molecular metabolism*. 2016; **5**: 352-365
- [51] Mookerjee SA, Goncalves RL, Gerencser AA, Nicholls DG, Brand MD. The contributions of respiration and glycolysis to extracellular acid production. *Biochimica et biophysica acta*. 2015; **1847**: 171-181

Table 1: Study subject characteristics

| | |
|---|------------------|
| Number of participants | 12 |
| Gender (male/female) | 3/9 |
| BMI in kg/m ² (mean and range) | 25.8 (20.7-37.9) |
| Age in years (median and range) | 62 (39-84) |
| Malignant disease/Benign disease | 2/10 |

Table legend

Gene expression analyses was performed on human adipose tissue biopsies collected from the neck area of patients admitted for elective neck surgery at Aarhus University Hospital.

Figure legends

Figure 1: Distribution of ¹¹C-metformin in wild-type mice.

A) Coronal T1-weighted MRI (T1W MRI) sequence, co-registration of T1W MRI and PET and Volumes of Interest (VOIs) in BAT. Scale bar to the right represents standard uptake value 0–0.7. B) Dynamic distribution of ¹¹C-metformin in the liver and BAT of FVB wild type mice, n=7. C) BAT-to-blood ratio AUC(0-60min). D) Murine metformin biodistribution one hour after intravenous injection. Relative Count per Minutes (CPM) in six C57BL/6 mice. No significant difference was found between CPM in BAT, Liver, intestines and kidney by ANOVA post hoc analyses. Data represent the mean +/- SEM. Error bars that are not visible are contained within the symbols. *: $P < 0.05$.

Figure 2: Distribution of ¹¹C-metformin in BAT.

A) Distribution in cimetidine pre-treated (n=5) and control mice (n=5). B) Distribution in OCT1/2^{-/-} (n=4) and Wild-Type mice (n=7). C) Distribution in pyrimethamine treated mice (n=4) and control mice (n=3). Data represent the mean + SEM. Error bars that are not visible are contained within the symbols. *: $P < 0.05$.

Figure 3: Gene expression analyses.

A) Uncoupling protein 1 (*Ucp1*) presence in brown adipose tissue (BAT) and subcutaneous inguinal tissues from mice (n=6) and in human (n=12) subcutaneous adipose tissue (SUBCU) deep neck adipose tissue (DNAT). Murine inguinal *Ucp1* expression is set at 1. B) Organic cation transporter 1-3 (*Oct1-3*), Multidrug and toxin extrusion protein 1 (*Mate1*) and Plasma membrane monoamine transporter (*Pmat*) transcription pattern in BAT, subcutaneous inguinal fat = ING, Liver, kidney, colon and ilium in mice (n=6). C) *OCT1-3*, *MATE1* and *PMAT* transcription in DNAT (n=24), SUBCU (n=12) and TERT-hBA cells (n=3). Data are shown as mean (+ SEM).

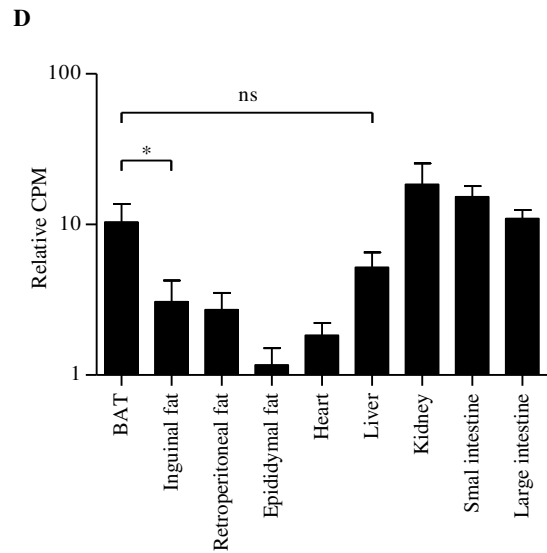
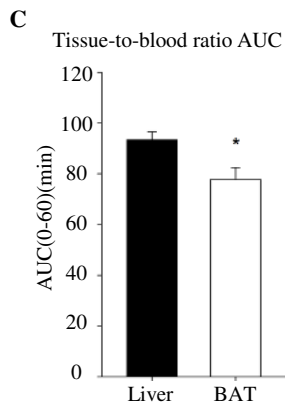
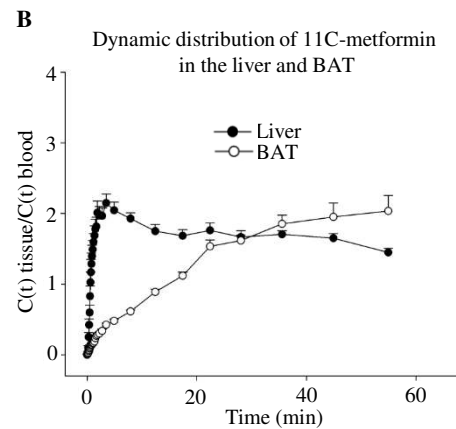
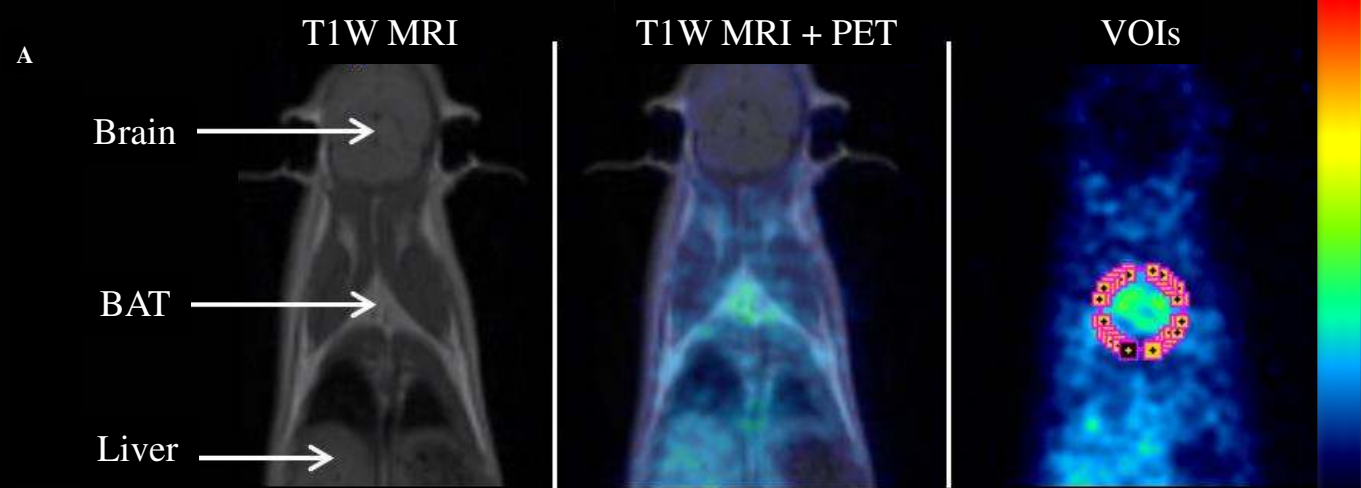
Figure 4: Human brown adipocyte (TERT-hBA) oxygen consumption and extracellular acidification rates during metformin incubation.

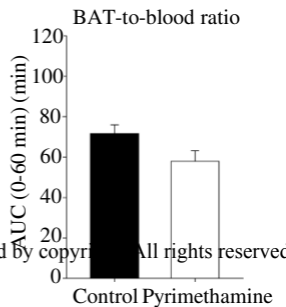
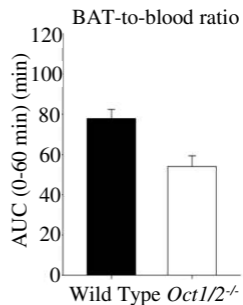
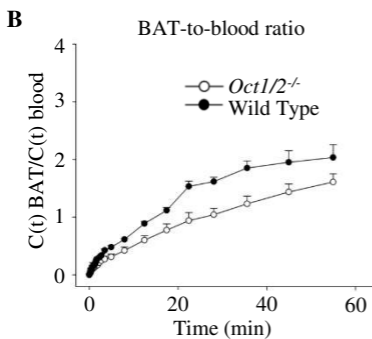
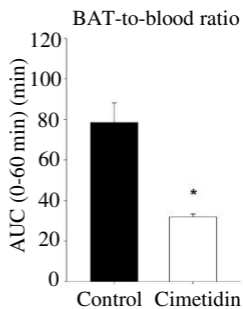
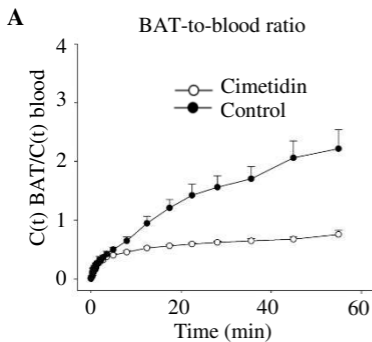
Illustration of the oxygen consumption rate (OCR) (A) and extracellular acidification (ECAR) (B) in control cells and metformin treated cells at various concentrations (n=1 with 10-15 replicates per intervention). Mean OCR (C) and ECAR (D) of control cells and metformin treated cells (1 mM) in three independent assessments. Cells were pretreated with metformin for one hour before the first measurement. Basal measurements were assessed at the last time point before adding the chemical uncoupler Carbonyl cyanide-4-(trifluoromethoxy)phenylhydrazone (FCCP). Uncoupled values were assessed at the last point before adding rotenone and antimycin A. OCR and ECAR values are

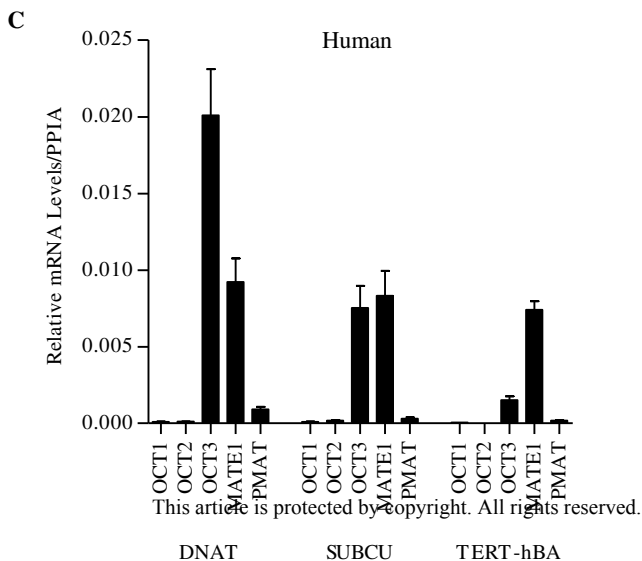
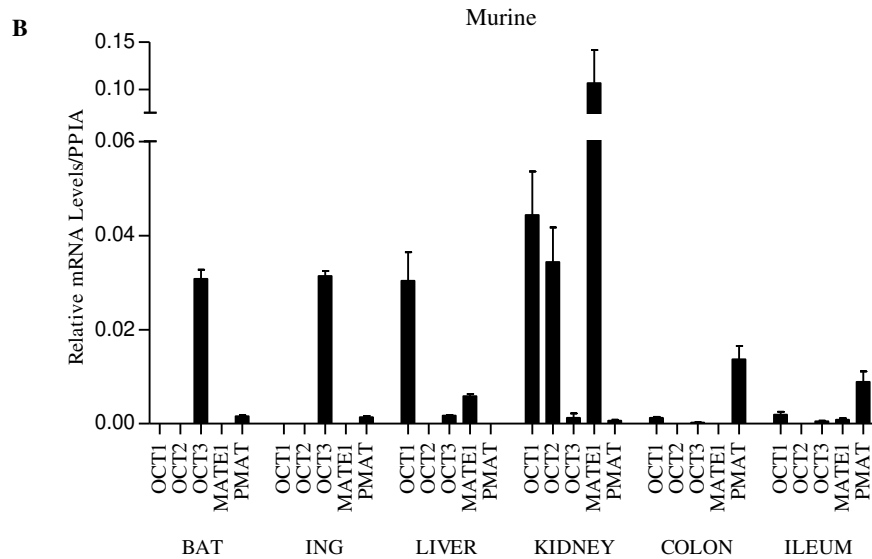
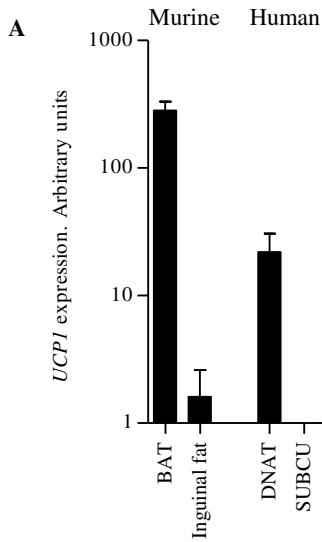
depicted relative to a mean of 100 for control cells. Data are shown as mean (\pm SEM). **: $P < 0.01$

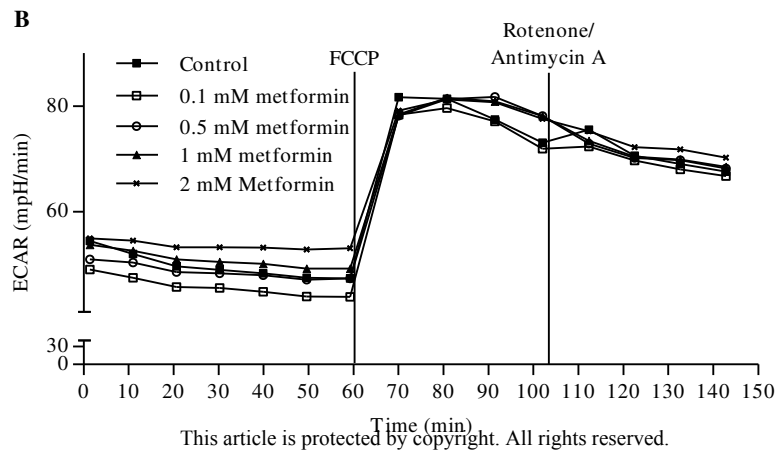
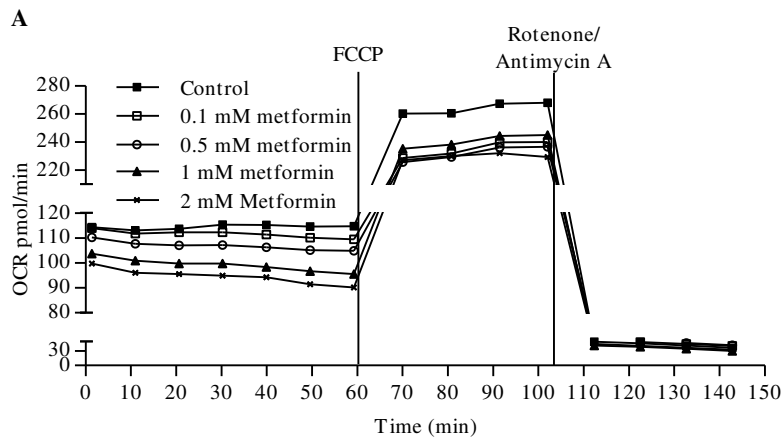
Figure 5. Human browned adipocytes exposed to prolonged metformin treatment.

The human cell lines hMADS (n=3) TERT-hWA (n=2) were converted to their beige phenotype and incubated with metformin 0.1 mM and 0.5 mM for 24 hours. A) oxygen consumption rate (OCR) and B) extracellular acidification rate (ECAR) under basal conditions and after chemical uncoupling by FCCP. As basal OCR and ECAR differed between the cell models, OCR is depicted as pct of control cells. *: $P < 0.05$. **: $P < 0.01$









This article is protected by copyright. All rights reserved.

